

Effect of the shear layer on the etching behavior of 6060 aluminum extrusion alloys

Lutz, Alexander; Lapeire, Linsey; Nguyen-Minh, Tuan; Verbeken, Kim; Terryn, Herman; De Graeve, Iris

DOI

[10.1002/sia.6632](https://doi.org/10.1002/sia.6632)

Publication date

2019

Document Version

Final published version

Published in

Surface and Interface Analysis

Citation (APA)

Lutz, A., Lapeire, L., Nguyen-Minh, T., Verbeken, K., Terryn, H., & De Graeve, I. (2019). Effect of the shear layer on the etching behavior of 6060 aluminum extrusion alloys. *Surface and Interface Analysis*, 51(12), 1251-1259. <https://doi.org/10.1002/sia.6632>

Important note

To cite this publication, please use the final published version (if applicable). Please check the document version above.

Copyright

Other than for strictly personal use, it is not permitted to download, forward or distribute the text or part of it, without the consent of the author(s) and/or copyright holder(s), unless the work is under an open content license such as Creative Commons.

Takedown policy

Please contact us and provide details if you believe this document breaches copyrights. We will remove access to the work immediately and investigate your claim.

Effect of the shear layer on the etching behavior of 6060 aluminum extrusion alloys

Alexander Lutz¹  | Linsey Lapeire² | Tuan Nguyen-Minh^{3,4} | Kim Verbeken² | Herman Terryn¹ | Iris De Graeve^{1,2}

¹Research Group Electrochemical and Surface Engineering, Vrije Universiteit Brussel, Brussels, Belgium

²Department of Materials, Textiles and Chemical Engineering, Ghent University (UGent), Ghent, Belgium

³Department of Materials Science and Engineering, Delft University of Technology, Delft, The Netherlands

⁴Department of Electrical Energy, Metals, Mechanical Constructions and Systems, Ghent University (UGent), Ghent, Belgium

Correspondence

Alexander Lutz, Research Group Electrochemical and Surface Engineering, Vrije Universiteit Brussel, Pleinlaan 2, Etterbeek, Brussels 1050, Belgium.
Email: alexander.lutz@vub.ac.be

Funding information

Fonds Wetenschappelijk Onderzoek; Vlaamse Agentschap Innoveren & Ondernemen, Grant/Award Numbers: 140710, HBC.2017.0300

The occurrence of preferential grain etching (PGE) during alkaline etching of aluminum extrusion alloys from the 6XXX series is often linked to the presence of certain impurity elements such as zinc, causing an undesired etching appearance. In the presented work, an additional culprit in this context is identified, which has not been investigated yet. A clear relation between PGE and the presence of a subsurface shear layer is identified for extruded Al 6060 alloys containing 0.02 and 0.06 wt% Zn. This shear layer can be distinguished from the bulk of the metal by its difference in crystallographic texture as visualized by electron backscatter diffraction (EBSD). For the Zn enriched alloy, the $\langle 111 \rangle$ //ND grains are etched away faster than grains with other orientations, resulting in the grainy appearance typical for PGE. Independent of the Zn content in the alloy, once the shear layer is removed and $\langle 111 \rangle$ //ND grains are practically absent on the new surface, the depth variations caused by preferential etching disappear. Instead, the surface of the alloy is attacked uniformly by the caustic etch bath.

KEYWORDS

aluminum alloys, EBSD, extrusion, preferential grain etching, shear layer

1 | INTRODUCTION

The production of goods made from recycled aluminum saves about 90% of CO₂ emissions and 95% of energy compared with ones made from primary aluminum. However, it comes with the disadvantage of enrichment of alloying elements like zinc, present in the recycling scrap. Zinc dissolves up to 2 wt% in the aluminum alloy and cannot be easily removed; it affects functional properties such as the appearance after etching and anodizing, which is crucial in certain applications such as in architecture. The etching prior to anodizing is applied as a cleaning step and to create a uniform matt finish, minimizing visible die lines or flow lines on mill-finished extrusion products. In the case of colored components, it can also affect the color.^{1,2}

As Dowell et al already stated in 1987, variations in the visual appearance can arise through variations in the etching conditions, difference in metal composition, or a combination of both.¹ When

nowadays, alloys are alkaline etched, the grain boundaries are typically attacked stronger than the grains because of a lower potential of the grain boundaries. This effect leads to a dull, matte appearance. However, in some cases, the surface can also have a spangling, grainy appearance similar to galvanized surfaces. This undesired effect is caused by preferential grain etching (PGE).^{3,4} PGE is an etching behavior where some grain orientations are etched away to a larger extent than others and surface planes of different heights and tilts are formed.⁵ Consequently, the reflectivity of the surface varies locally, and the appearance is no longer homogeneously dull. One of the main reasons for this effect is the presence of Zn in the alloy as well as in the alkaline etching bath.^{1,3,4,6,7} Increased amounts of Zn are thought to amplify the surface reactivity of certain grains with respect to other grains. Thus, the grain orientation plays an important role on the etching depth. Gentile et al showed by Rutherford backscattering spectroscopy that Zn enrichment during etching depends on the grain

orientation.⁸ Chandia et al⁶ assumed that the {100} planes are the most highly Zn enriched planes during etching. They reason that this enrichment of Zn will make the {100} planes more cathodic as compared with {110} and {111} planes causing a microgalvanic coupling between the differently oriented grains. It is proposed that as well, the Zn content in the etching solution as well as in the alloy itself can play a crucial role.^{6,7} Holme et al³ concluded from their electron backscatter diffraction (EBSD) and secondary ion mass spectroscopy results that the deepest <111>//ND grains have more near-surface Zn than other grains after alkaline etching. However, their hypothesis is based on the occurrence of Zn enrichment by selective dissolution of the active Al component. A consensus on the origin of the PGE and the link with the Zn content of the alloy is not yet reached.⁷

The amount of Zn in 6060 alloy specifications is limited to 0.15 wt%. Many companies choose to work with an even lower level of 0.03 wt%—a limit below which PGE usually does not occur. However, the reduction of Zn in recycled 6000 series alloys is difficult and expensive. Industrial etching solutions contain so-called zinc catchers to remove Zn by precipitation in the etching bath.⁹ It is worth mentioning, that in 7000 alloys, Zn is deliberately added at a much higher level than in the 6000 alloys to form hardening phases together with Mg. However, those alloys generally do not have a grainy surface appearance after etching. Hence, why 6000 alloys are so sensitive to PGE is not yet fully understood. The authors of this study investigated an additional mechanism for the case of Al 6060 that can also cause PGE in order to draw a clearer mind map of the reasons for PGE.

The objective of this study is to investigate the alkaline etching response of two industrially extruded Al 6060 alloys, one with a low Zn content of 0.02 wt% and one with a higher Zn content of 0.06 wt%. By EBSD, the microstructure and crystallographic texture of both extruded profiles will be characterized, and their microstructure

will be related to the corresponding etching behavior of the extrusion profiles.

2 | MATERIALS AND METHODS

2.1 | Materials

The 6060 alloys investigated in the present work were produced and extruded by EMAX nv, Belgium. The compositions of alloy A and B are very similar and given in Table 1. Alloy A has a Zn concentration similar to a primary alloy, and alloy B is enriched in Zn to simulate a recycled Zn rich 6060 alloy.

Before extrusion, the billets were heat treated to homogenize the microstructure. The heat treatment involves the formation of α -AlFeSi^{10,11} and the dissolution of Mg₂Si particles into the matrix. This heat treatment also assures the uniform distribution of alloying elements in the matrix. After this homogenization step, both alloy A and alloy B were reheated to 480°C and extruded at the speed of 27.5 m/min. Samples are then cooled by forced air and artificially aged to T5 (195°C for 5 hours).

2.2 | Alkaline etching

Samples of about 1 cm² were cut from of the extrusion profiles. The samples were degreased, followed by alkaline etching and acid desmutting, with intermediated water rinsing. The various steps of the pretreatment are listed in detail in Table 2. To investigate the alkaline etching behavior of the alloy deeper in the sample, 25 ± 2 and 200 μm of the outer surface were ground away with 1200 SiC paper, thus probing either the shear layer or the bulk of the extrusion profile, respectively.

2.3 | Electron backscatter diffraction

For the microstructural observations, EBSD was used. EBSD observations of the two Al alloys were made at identical positions in the profile sample, ie, on the extrusion plane containing the normal direction (ND) and transverse direction (TD) (Figure 1A) and on the normal plane containing the extrusion direction (ED) and the TD (Figure 1B).

TABLE 1 Composition of alloy A and alloy B

	Si, wt%	Fe, wt%	Cu, wt%	Mn, wt%	Mg, wt%	Cr, wt%	Zn, wt%
Alloy A	0.45	0.20	0.015	0.055	0.375	0.02	0.02
Alloy B	0.45	0.25	0.015	0.055	0.375	0.02	0.06

TABLE 2 Parameters for the surface pretreatment

Step	Treatment	Medium	Time	Temperature
1	Degreasing	Acetone	Dip	RT
2	Etching	50 g/L NaOH (500 ml)	13 min	60°C
3	Rinsing	Deionized water	1 min	RT
4	Desmutting	10 vol% HNO ₃	1 min	RT
5	Rinsing	Deionized water	1 min	RT
6	Rinsing	Acetone	Dip	RT

Abbreviation: RT: room temperature.

Crystallographic orientation data of each measurement were used to calculate textures by the spherical harmonic expansion with the highest term of the harmonic series of 16 and a half width of the Gaussian spread of 5° . The representation of the crystallographic texture is done by means of orientation distribution functions (ODFs), a series of two-dimensional sections (Φ_1 , Φ) of the three-dimensional space of the Euler angles (Φ_1 , Φ , Φ_2). Euler angle $\Phi_2 = 0^\circ$, 45° , and 65° is indicated under each section. The ODF is shown as a color intensity plot. Important orientations and fibers are marked in the $\Phi_1 = 0^\circ$ to 90° ODF section. The orientation images are represented in this study as inverse pole figure (IPF) maps, ie, the color of each

grain represents the crystal orientation parallel to the specified direction. To obtain a suitable surface for EBSD measurements, the samples were mechanically ground and polished down to 1- μm diamond paste (Struers), followed by a finishing electropolishing step (48 V, 4 seconds) with the Lectropol-5 (Struers) in a perchloric acid electrolyte (A2, Struers). The EBSD system was attached to a Quanta FEI field emission scanning electron microscope (FE-SEM) operated at 20 kV. Measurements were carried out with a step size of 1 to 3 μm depending on the sample grain size, and the orientation data were post-processed with the commercial orientation imaging software OIM-TSL. For texture analysis, in order to obtain a statistically reliable texture representation, several scans were stitched together with a minimum of 1.1 mm^2 per investigated area. A tolerance of 10° from the ideal orientation is used to determine the volume fraction of the $\langle 111 \rangle // \text{ND}$ grains.

The Quanta FEI FE-SEM in secondary electron (SE) image mode was also used to visualize the surface of the profiles after alkaline etching.

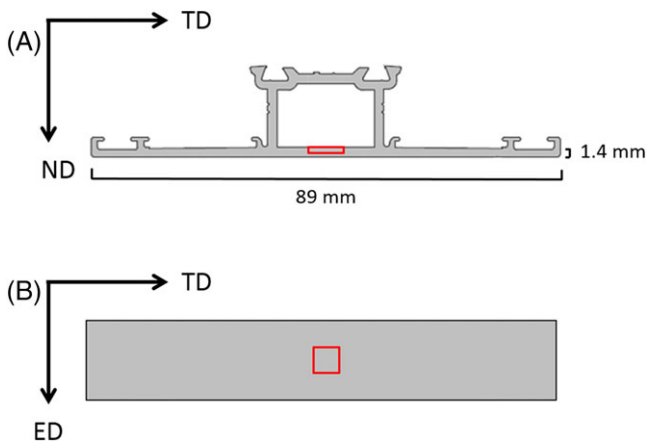


FIGURE 1 Schematic overview of the extrusion profiles of alloy A and alloy B of A, the cross section (normal direction [ND]-transverse direction [TD]) and B, the normal plane (extrusion direction [ED]-TD). In red the positions of the electron backscatter diffraction (EBSD) measurements

3 | RESULTS

3.1 | Microstructural investigation

Figure 2 shows the IPF maps of the cross section (extrusion plane) of alloy A and B. Both the ND and the ED IPF maps are shown for clarity. Although it is not pronounced in the ND IPF map, when looking at the ED IPF map, a clear distinction in crystallographic orientation can be made between the bulk of the extrusion profile and the surface for both alloys. The thickness of the surface layer, based on the difference in crystallographic orientation, is measured for both alloys on several

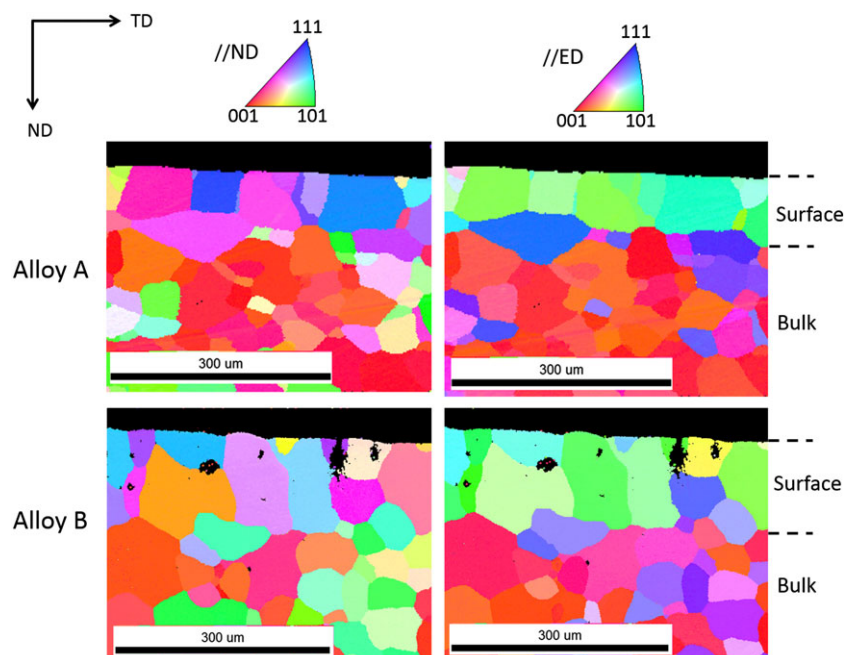


FIGURE 2 Normal direction (ND) and extrusion direction (ED) inverse pole figure (IPF) maps of alloy A and alloy B

scans, and a notable difference is observed. For alloy A, the thickness of the surface layer is $75 \pm 11 \mu\text{m}$, and for alloy B, the thickness is $126 \pm 14 \mu\text{m}$ (average of 35 measurements on different length positions of the extrusion profile). The grain size of the surface layer on the ED-TD plane, determined with the linear intercept method, is $46 \pm 15 \mu\text{m}$ for alloy A and $57 \pm 23 \mu\text{m}$ for alloy B.

The grain orientation in the surface layer as well as in bulk was analyzed by EBSD and compared based on the volume fraction of $\langle 111 \rangle // \text{ND}$ grains. Figure 3 shows that in the surface layer, the volume fraction of $\langle 111 \rangle // \text{ND}$ grains is 8.2% and 6.9% in alloy A and B, respectively. In the bulk, the volume fractions of these grains are less than 0.1% for both alloys. Interestingly, the volume fraction varies only slightly between alloy A and alloy B, but there is a factor 100 difference between their presence in the shear layer and the bulk grains.

To determine the texture of the surface layer, several EBSD scans were made on the ED-TD surface (normal plane). The texture of the bulk was extracted out of several ND-TD (extrusion plane) scans. In

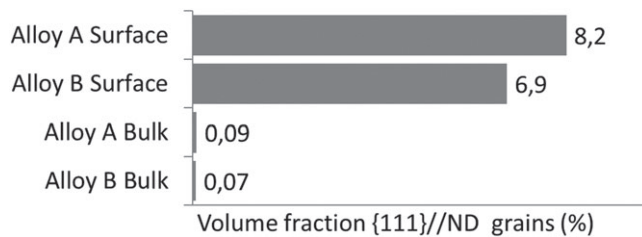


FIGURE 3 Volume fraction of $\langle 111 \rangle // \text{ND}$ grains in the bulk and surface layer of alloy A and alloy B

Figure 4 the ODFs of alloy A and alloy B are given for both the bulk of the material and the surface layer; no sample symmetry was imposed.

3.1.1 | Surface

Although Ihara et al stated that the surface layer of an extruded Al alloy has an orientation distribution, which is relatively random,¹² a more textured surface microstructure is observed in our case. The Zn lean (alloy A) and Zn rich (alloy B) alloys have a maximum intensity of $21\times$ random and $18\times$ random, respectively.

Remnants of the $\langle 110 \rangle // \text{ED}$ -fiber and components of the γ -fiber ($\langle 111 \rangle // \text{ND}$) can be identified in the measured surface texture. These are typical texture components of face centered cubic (FCC) crystals in shear deformation. Also, the rotated cube component $\{001\} \langle 110 \rangle$ (part of the $\langle 110 \rangle // \text{ED}$ -fiber) is associated with shear deformation in FCC metals. Higher intensities close to this component are identified in the surface texture of alloy A and alloy B. To further relate the measured surface texture to the texture of a FCC metal after shear deformation, the surface texture is compared with a modelled FCC shear texture (Figure 5). For the modelling of the shear deformation texture, the visco-plastic self-consistent (VPSC) model is used. The initial texture is assumed to be random, and the total equivalent strain (ϵ_{VM}) is 0.7. However, the simulated deformation texture is not completely similar to the measured surface texture. This is because of the recrystallization process, which takes place during or after extrusion and which is not considered in the crystal plasticity simulation. During recrystallization, among all grains of the deformation microstructure, only crystals having low stored energy and a grain

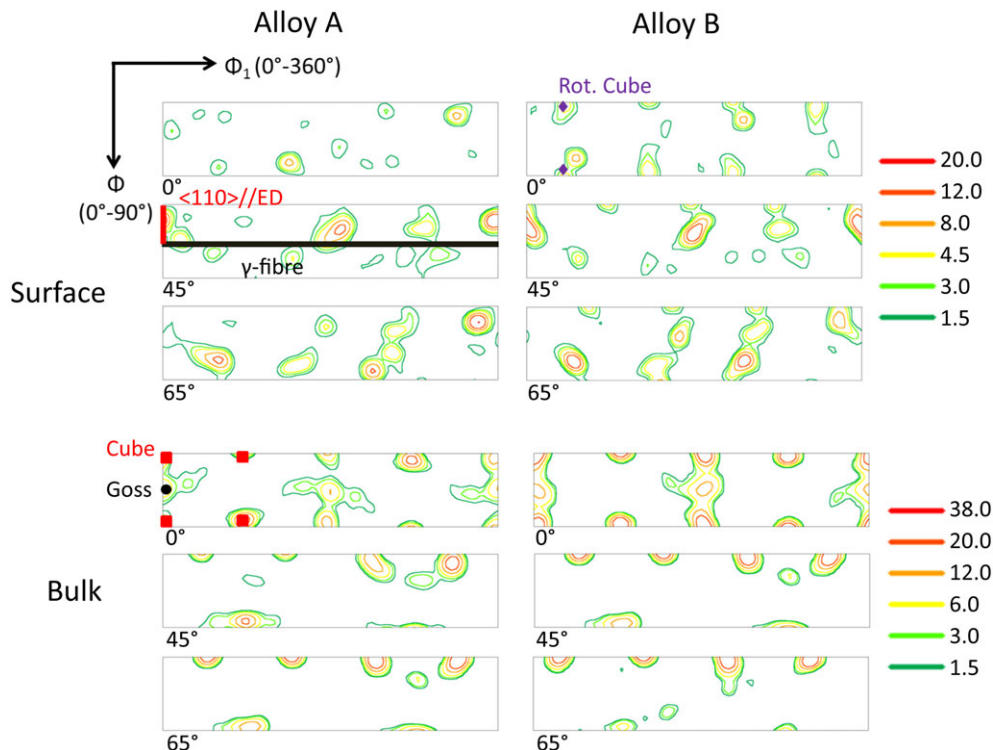


FIGURE 4 Orientation distribution function (ODF) sections (with $\Phi_2 = 0^\circ, 45^\circ, 65^\circ$) of the surface and bulk texture of alloy A and alloy B

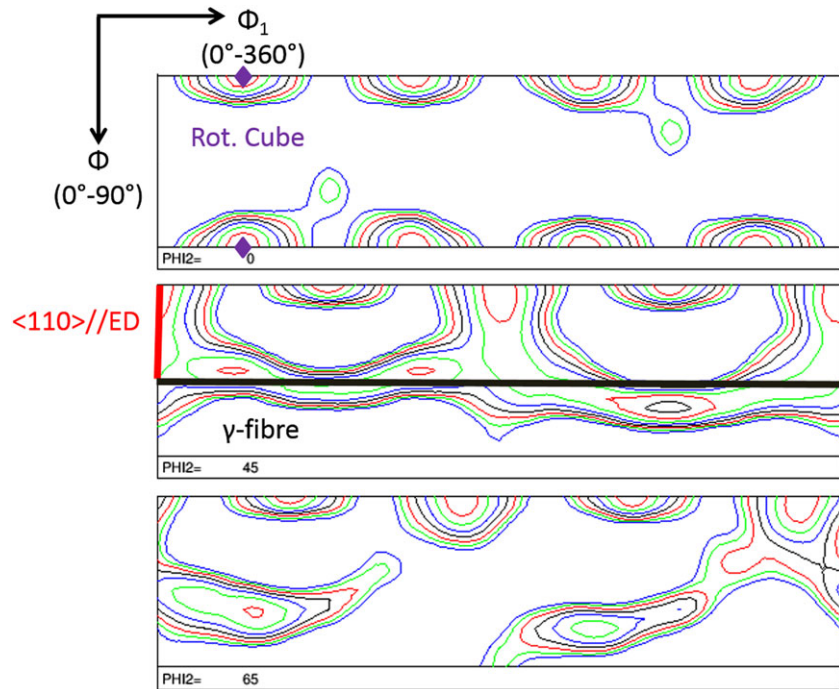


FIGURE 5 Orientation distribution function (ODF) sections (with $\Phi_2 = 0^\circ, 45^\circ, 65^\circ$) of the calculated face centered cubic (FCC) crystals under simple shear deformation

boundary of $\langle 111 \rangle 40^\circ$ to the deformation matrix have a chance to nucleate and grow.

3.1.2 | Bulk

The bulk crystallographic texture is in both alloys very typical for FCC materials with a recrystallized microstructure deformed by plane strain compression.¹³ The maximum intensities are observed in the cube component $\{001\}\langle 100 \rangle$ and goss component $\{011\}\langle 100 \rangle$ for both alloys, with a maximum intensity for alloy A of $31\times$ random and $37\times$ random for alloy B. However, for both alloys, the cube and goss component are somewhat rotated around TD.

3.2 | Effect of alkaline etching on surface layer

The SE image on the normal plane of alloy A (with low amount of Zn) taken after alkaline etching of the sample shows the typical surface morphology (Figure 6A). For this alloy, the main attack is at the grain boundary; this is typically related to the disturbed crystal structure and elemental deficiency zones at and next to the grain boundaries.¹⁴ This surface gives the desired matt finish of the Al extrusion profile. Comparing the ED IPF map obtained after etching (Figure 6B) with the ED IPF map of the cross section (Figure 2 Alloy A//ED) reveals that the outer surface after etching is still located inside the shear or surface layer of the material.

The SE image of the surface of alloy B shows a completely different etching morphology (Figure 7A). In this case, certain grains are significantly more attacked than others, resulting in the grainy morphology and nonhomogeneous visual appearance. Similar with alloy A, the exposed surface after alkaline etching of alloy B (higher Zn content) is also still located in the shear layer (Figure 2 Alloy B//ED and Figure 7B).

In Figure 8, an alkaline etched zone of alloy B is displayed, with the corresponding ND IPF map. In this orientation, the preferentially etched grains are clearly distinguishable from the others. The white stars mark two of those grains in the SE image and on the IPF map. An orientation analysis of all visually attacked grains in the SE image shows that all grains with an orientation close to $\langle 111 \rangle // \text{ND}$ are preferentially etched.

3.3 | Effect of alkaline etching on ground surface layer

In this experiment, the alkaline etching is performed after removal (by grinding with 1200 SiC paper) of about $25 \mu\text{m}$ of the outer surface, exposing a surface that is still inside the shear layer. This experiment is done to rule out that the previously observed differences are related to possible outer surface contaminations or roughness differences. In Figure 9, the SE image after alkaline etching of alloy A (Figure 9A) and alloy B (Figure 9B) is shown. Similar to the etching response of alloy A and alloy B without prior grinding (Figures 6A and 7A), alloy A shows grain boundary attack, while alloy B shows PGE.

3.4 | Effect of alkaline etching on bulk layer

To investigate the etching response of the bulk of the material, for both alloys more than $200 \mu\text{m}$ is removed by grinding, thus removing the identified shear or surface layer completely and exposing a surface consisting of the bulk structure of the metal. In this case, the etching morphologies look less pronounced and homogenous for both alloy A (Figure 10A) and alloy B (Figure 10B). For alloy A, weak grain boundary attack is visible. For alloy B, a more uniform attack can be observed with hardly any visible PGE effects.

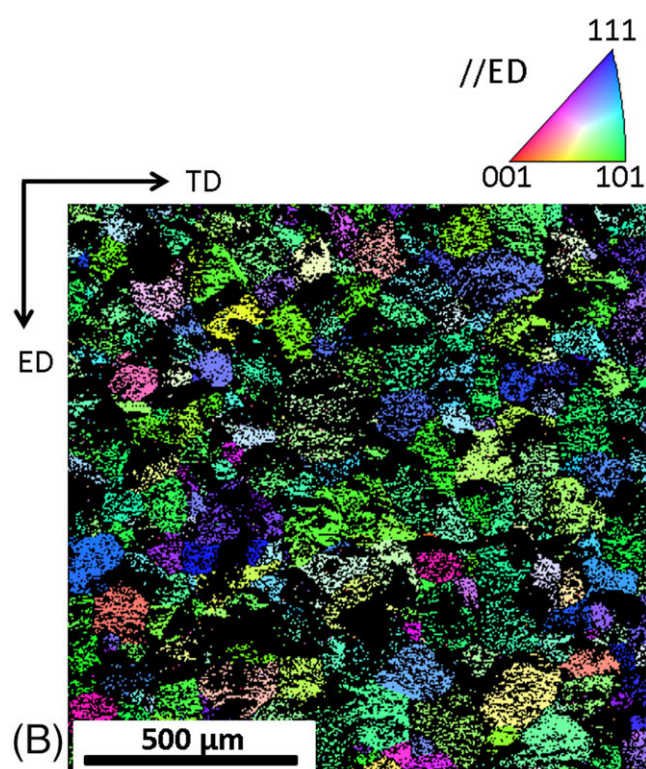
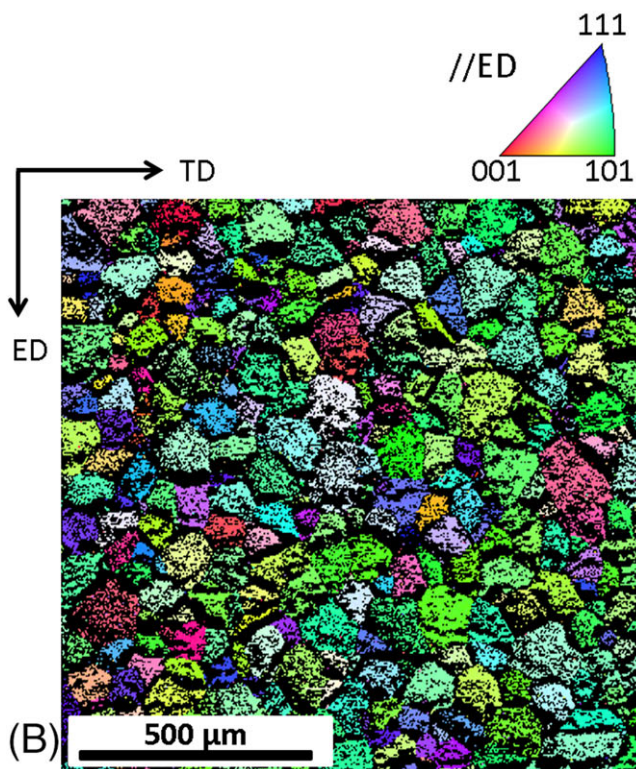
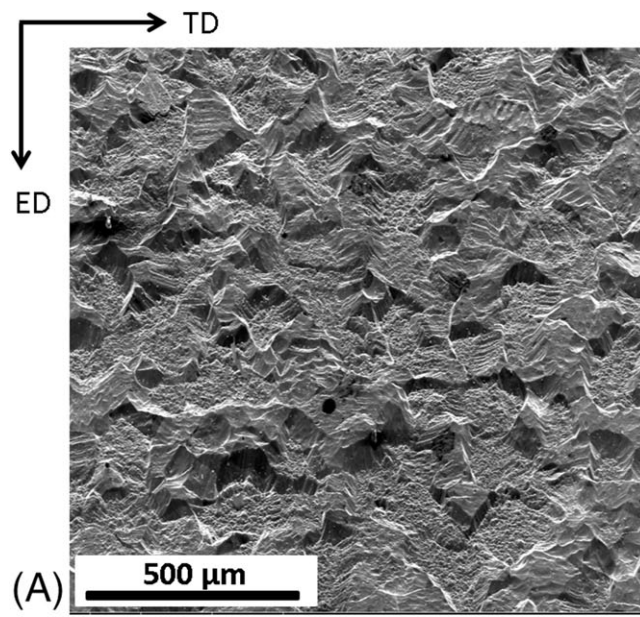
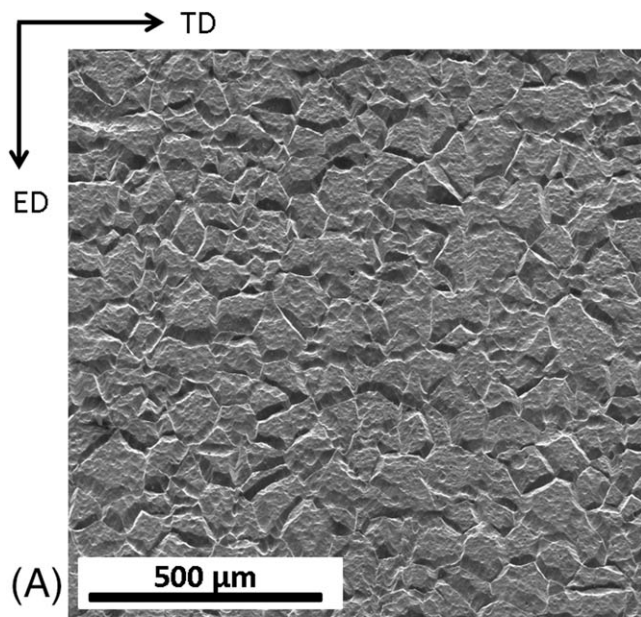


FIGURE 6 Alloy A: A, Secondary electron (SE) image after alkaline etching on the normal plane and B, extrusion direction (ED) inverse pole figure (IPF) map after alkaline etching on the normal plane

FIGURE 7 Alloy B: A, Secondary electron (SE) image after alkaline etching on the normal plane and B, extrusion direction (ED) inverse pole figure map after alkaline etching on the normal plane

4 | DISCUSSION

4.1 | Microstructure of the extruded alloy A and alloy B

Since extrusion is a nonhomogeneous deformation process, variations of microstructure and texture over the profile cross-section can be

expected and are observed in Figure 2 for both alloy A and alloy B. In both alloys, a bulk structure and a surface layer were identified and distinguished from each other by their difference in crystallographic orientation, as can be seen in the orientation data in the ED IPF map. The textures of the surface layer and the bulk have been characterized by EBSD investigations of these specific zones. In the texture of the recrystallized surface layer of both alloys (Figure 4), some resemblance can be found with the modelled FCC shear texture

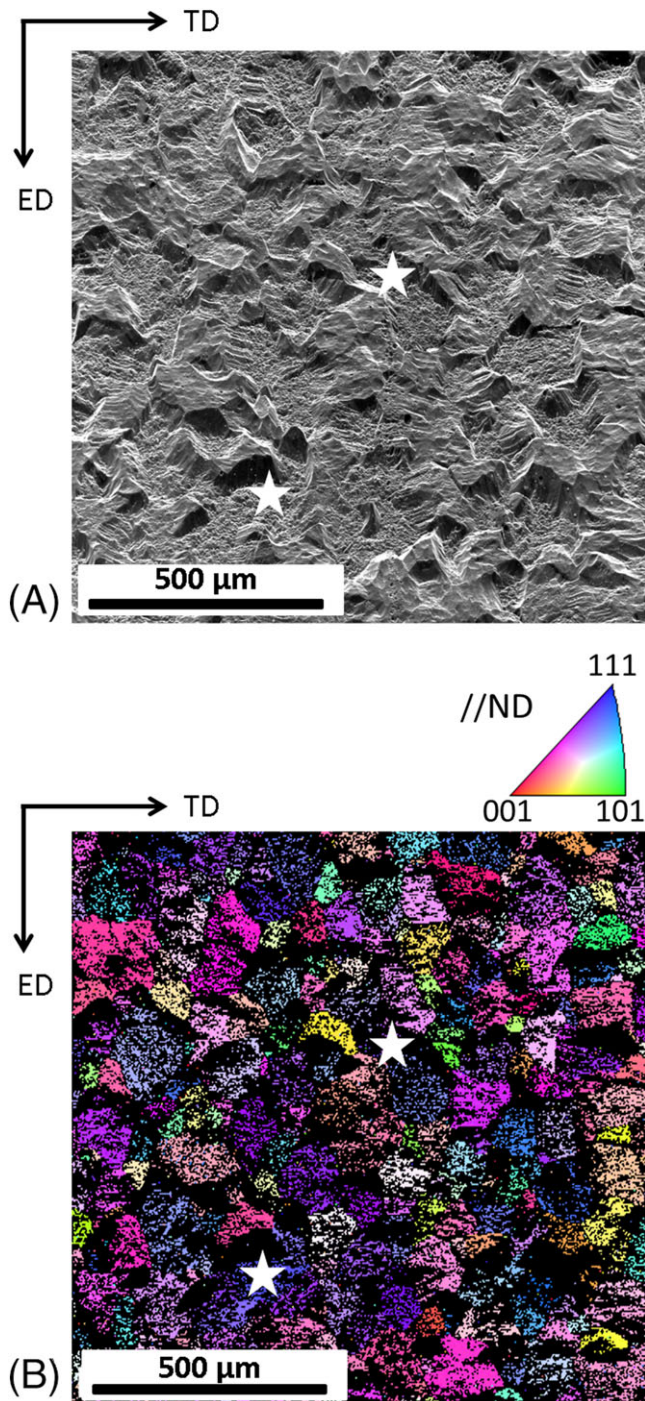


FIGURE 8 A, Secondary electron (SE) image and B, corresponding normal direction (ND) inverse pole figure map on the ND plane of alloy B after alkaline etching

(Figure 5). In the modelled shear texture, the typical texture components of shear deformation are observed, namely, the $\langle 110 \rangle // ED$ -fiber and the γ -fiber. In the measured shear texture, only remnants of the $\langle 110 \rangle // ED$ -fiber and the γ -fiber can be found, which this is due to the recrystallization process that occurs during or after extrusion. Also, a texture component near the rotated cube $\langle 001 \rangle \langle 110 \rangle$ is observed in the measured surface texture. This rotated cube

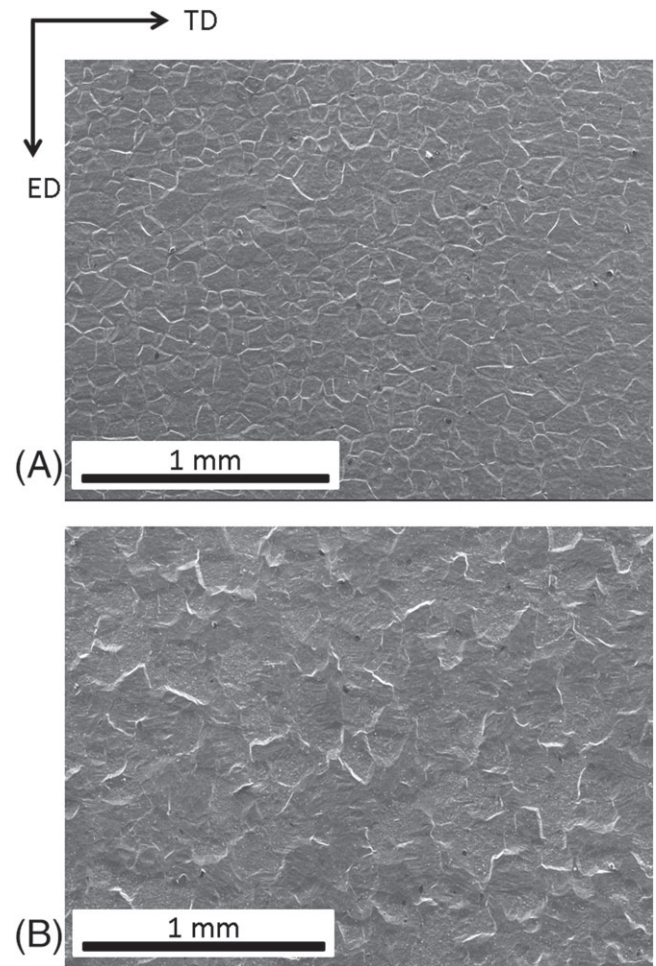


FIGURE 9 Secondary electron (SE) image on the normal plane of A, alloy A and B, alloy B after alkaline etching of the ground surface

component is formed during shear deformation and is retained during recrystallization. This proves the presence of shear in the surface layer of extruded profiles. The presence of the shear layer in the extruded profiles can be explained as follows. During extrusion, the billet surface experiences adhesive friction against the die wall, while the core of the billet is pushed forward through the die by the advancing ram. In this way, a shear zone forms between the core material and the peripheral surface layer due to different local forces acting on the material. For alloy A and alloy B, a small intensity difference is observed in this shear layer: $21\times$ random and $18\times$ random, respectively.

Another noticeable difference between both alloys is the thickness of this shear layer (75 ± 11 and $126 \pm 14 \mu\text{m}$, respectively). However, this observation is not conclusive and must be verified, as the microstructure development of extruded profiles not only varies along the cross section but also along the extrusion length.¹⁵ To confirm this observation, samples must be taken for both alloys at the same length position of the full extrusion profile, which was not possible for the current samples.

In the bulk of both alloy A and alloy B, a strong cube texture that is somewhat rotated around the TD can be seen. The cube texture is the

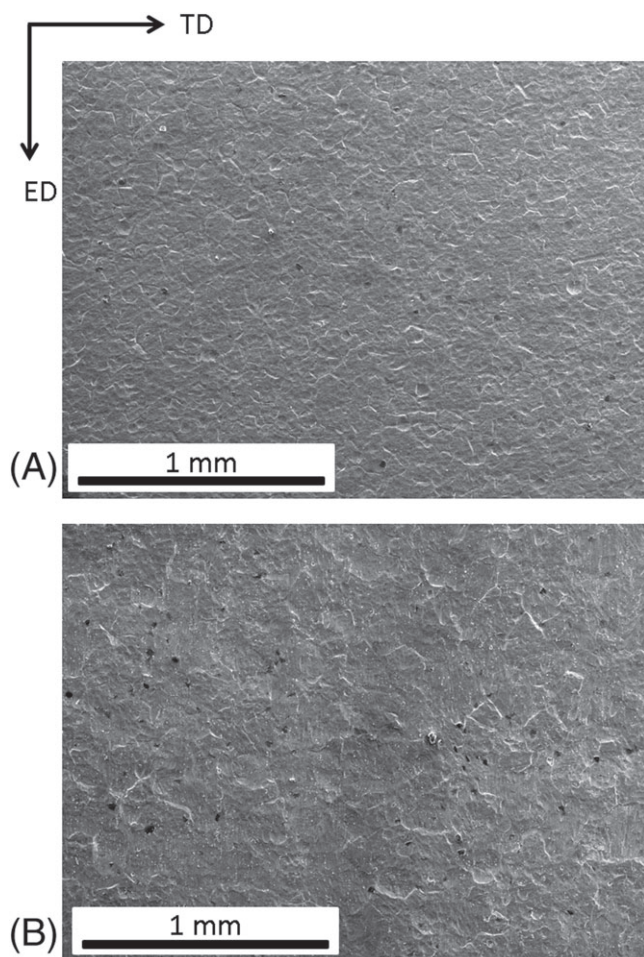


FIGURE 10 Secondary electron (SE) image on the normal plane of A, alloy A and B, alloy B after alkaline etching of the bulk of the material

typical texture component that is present in FCC metals after plane strain compression and recrystallization. A material with a perfect plane strain texture will have symmetrical crystallographic orientation both in ED and TD. The rotation around TD is due to a small shear deformation on top of the plane strain compression present in the bulk of the material.

4.2 | Link between microstructure and alkaline etching behavior

Three different experiments were conducted to investigate whether the difference in alkaline etching response of low-Zn Al 6060 (alloy A, showing grain boundary etching) and Zn enriched Al 6060 (alloy B, showing PGE) is purely a bulk feature or if it is also related to the surface layer.

In the first experiment, the alkaline etching procedure was executed according to industrial practice, ie, on the bare surface. The second experiment was conducted to verify to which extent the different etching behaviors of the investigated alloys are related to possible differences in roughness or top layer impurities due to the extrusion process. For this purpose, the outer surface is removed (about 25 μm)

before applying the alkaline etching treatment. In the third experiment, the shear layer is completely removed by mechanical grinding and thereby exposing a surface inside the bulk of the alloys to the alkaline etching solution.

The results of the first experiment (Figures 6 and 7) confirm the observations reported in literature on the two different etching effects. The Zn lean alloy (Figure 6) was attacked preferentially at the grain boundaries, giving the desired surface finish before anodizing.¹ The Zn rich alloy has a grainy surface appearance (Figure 7) caused by different etching rates for different grains and subsequently giving the material a terrace-like surface topography similar as described by Koroleva et al.⁴ With use of the corresponding IPF map determined by EBSD (Figure 8), it is concluded that grains with the $\langle 111 \rangle$ direction parallel to the normal of the surface etch at a higher rate than the other orientations. For both alloys, it is shown that the etched surfaces are still part of the shear layer of the material (Figures 2, 5B, and 7B). The etched surfaces of the second experiment (Figure 9) demonstrate that removing the top surface before alkaline etching has no influence on the resulting etching response. For alloy A, grain boundary attack is still the main etching mechanism, whereas it is PGE for alloy B.

Finally, the third experiment reveals a different etching behavior in the bulk compared with the etching results of the shear layer (Figure 10). Alloy A shows a much less pronounced etching attack, although the main etching mechanism is still grain boundary attack. Alloy B shows practically no PGE anymore, but a generally rougher surface than the one of alloy A. For both alloys, this weakened etching behavior can be related with the bulk texture. Since the bulk material is heavily textured indicating that the grains have a preferred orientation, the amount of grain boundaries with a high level of misorientation is low. Typically, the most misoriented interfaces are more susceptible to grain boundary attack.¹⁶ Therefore, the grain boundary attack of alloy A during alkaline etching is gentler in the bulk. Alternatively, the PGE effect of alloy B strongly depends on the presence of $\langle 111 \rangle // \text{ND}$ grains who have the highest etching rate. Figure 3 shows that almost no $\langle 111 \rangle // \text{ND}$ grains are present in the bulk for preferential dissolution. The absence of these grains leads to a more evenly distributed attack.

Therefore, it can be concluded that the shear layer (and more specifically the texture of the shear layer) of the extruded profile can have a dominant influence on the different alkaline etching behavior of the Zn lean and the Zn rich Al 6060 alloys. When this shear layer is removed prior to etching, for example, by grinding or by adapting the extrusion process parameters, the difference in etching behavior between the Zn lean and Zn rich alloys is reduced. However, to get a better understanding on why the response of the shear layer to alkaline etching changes from grain boundary attack to PGE, dependent on the Zn level in the 6060 alloys, further investigations are necessary.

5 | CONCLUSION

In this work, two industrially extruded Al 6060 profiles are investigated, a Zn lean alloy (alloy A) and a Zn enriched alloy (alloy B). These

alloys have a completely different surface etching behavior although their composition hardly varies. Alloy A gives rise to grain boundary etching, while alloy B is prone to PGE. After a detailed EBSD observation of both extruded alloys in cross-section, a shear layer can be identified based on the crystallographic orientation of the grains, clearly distinguishing it from the alloy bulk structure. The results show that the difference in etching response is big between the Zn lean and the Zn enriched Al 6060 alloy within the shear layers, but is negligible in the bulk of the alloys. Removing the shear layers of the extruded profiles thus reduces the difference between the two etching behaviors. Hence, it can be concluded that the reasons for the different etching behavior of the Zn lean and Zn rich Al 6060 extrusion alloys must also be found in the properties of the shear layer and are not purely depending on the etching bath, the bulk structure, or composition of the alloys.

ACKNOWLEDGEMENTS

The authors wish to thank the Fonds Wetenschappelijk Onderzoek (FWO) and the Vlaams Agentschap Innoveren en Ondernemen (VLAIO) for funding this research (grant numbers 140710 and HBC.2017.0300).

CONFLICT OF INTEREST

The authors declare that they have no conflict of interest.

ORCID

Alexander Lutz  <https://orcid.org/0000-0003-0676-5170>

REFERENCES

- Dowell AJ. Metal structure and composition effects in the alkaline etching of aluminium. *Trans IMF*. 1987;65(1):147-151. <https://doi.org/10.1080/00202967.1987.11870791>
- Røyset A, Aukrust T, Holme B, Lein JE, Lunder O, Kolås T. Visual appearance characteristics of industrial aluminium surfaces. *Mater Today Proc*. 2015;2(10):4882-4889. <https://doi.org/10.1016/j.matpr.2015.10.041>
- Holme B, Ljones N, Bakken A, et al. Preferential grain etching of AlMgSi (Zn) model alloys. *ECS Trans*. 2010;25(40):71-79. <https://doi.org/10.1149/1.3496068>
- Bakken A. Effect of texture and Zn content on etch morphology of the aluminium alloy EN-AW 6063. s.
- Koroleva EV, Thompson GE, Skeldon P, Noble B. Crystallographic dissolution of high purity aluminium. *Proc R Soc a Math Phys Eng Sci*. 2007;463(2083):1729-1748. <https://doi.org/10.1098/rspa.2007.1846>
- Chandia MUF, Bauger Ø, Furu T. Effect of composition, grain size and texture on the etching response of 6xxx alloys. In: *Proceedings of the 12th International Conference on Aluminium Alloys*. Yokohama; 2010:781-786.
- Bauger Ø, Bjerkaas H. Aspects of preferential grain etching during alkaline pre-etching step before anodizing of aluminum profiles. In: *Proceedings of the Tenth International Aluminum Extrusion Technology Seminar*; 2012:421-430.
- Gentile M, Koroleva EV, Skeldon P, Thompson GE, Bailey P, Noakes TCQ. Influence of grain orientation on zinc enrichment and surface morphology of an Al-Zn alloy. *Surf Interface Anal*. 2010;42(4):287-292. <https://doi.org/10.1002/sia.3147>
- Newman KW, Atkins DC, Douglas GS. *Process for etching aluminum alloy surfaces*. 1957.
- Asensio-Lozano J, Suárez-Peña B, Vander VGF. Effect of processing steps on the mechanical properties and surface appearance of 6063 aluminium extruded products. *Materials (Basel)*. 2014;7(6):4224-4242. <https://doi.org/10.3390/ma7064224>
- Kuijpers NCW, Kool WH, Koenis PTG, Nilsen KE, Todd I, Van der Zwaag S. Assessment of different techniques for quantification of α -Al (FeMn)Si and β -AlFeSi intermetallics in AA 6xxx alloys. *Mater Charact*. 2002;49(5):409-420. [https://doi.org/10.1016/S1044-5803\(03\)00036-6](https://doi.org/10.1016/S1044-5803(03)00036-6)
- Ihara K, Shikama T, Morita K. Effect of extrusion temperature on recrystallization textures of extruded AA6005C alloys. *R D Res. Dev. Kobe Steel Eng. Reports*. 2012;62(2):43-47.
- Humphrey J, Hatherly M. *Recrystallization and Related Annealing Phenomena*. Elsevier; 2004 <https://doi.org/10.1016/B978-0-08-044164-1.X5000-2>.
- Larsen MH, Walmsley JC, Lunder O, Mathiesen RH, Nisancioglu K. Intergranular corrosion of copper-containing AA6xxx AlMgSi aluminum alloys. *J Electrochem Soc*. 2008;155(11):C550. <https://doi.org/10.1149/1.2976774>
- Valberg HS. *Applied Metal Forming: Including FEM Analysis*. New York: Cambridge University Press; 2010.
- Yang W, Ji S, Li Z, Wang M. Grain boundary precipitation induced by grain crystallographic misorientations in an extruded Al-Mg-Si-Cu alloy. *J Alloys Compd*. 2015;624(March):27-30. <https://doi.org/10.1016/j.jallcom.2014.10.206>.

How to cite this article: Lutz A, Lapeire L, Nguyen-Minh T, Verbeken K, Terryn H, De Graeve I. Effect of the shear layer on the etching behavior of 6060 aluminum extrusion alloys. *Surf Interface Anal*. 2019;51:1251-1259. <https://doi.org/10.1002/sia.6632>